Centre for Biotechnology
Department of Biosciences at Novum
Karolinska Institutet, Stockholm, Sweden

NON-ENVELOPED VIRUS INFECTION PROBED WITH HOST CELLULAR MOLECULES: A STRUCTURAL STUDY

Li Xing

Stockholm 2002

Published and printed by Karolinska University Press
Box 200, SE-171 77 Stockholm, Sweden

ISBN 91-7349-289-2

Dedicated to my parents

ABSTRACT

Early steps in virus replication require binding of the virus to its target cell, entry into the cell, and delivery of the viral genome into the cell in order to gain access to the cellular macromolecular synthesis machinery. This infectious process can only be initiated if the virus successfully attaches to a specific receptor on the plasma membrane of the target cell. Receptor specificity is one important factor for determining the target cell tropism of a virus.

Picornaviruses are a group of small non-enveloped viruses belonging to a well-characterized virus family. The prototypic picornavirus consists of a single-stranded positive-sense RNA molecule that is encased by a protein capsid approximately 50Å thick and 300Å in diameter. The capsid is composed of 60 copies of four virus proteins, arranged in a T=1 icosahedral lattice. The three larger proteins (VP1-3) form the outer surface and share a common eight-antiparallel-beta-barrel structural motif. The smallest viral protein (VP4) is located at the interface between the capsid protein and viral genomic RNA. The canyon, the surface depression around each of the twelve icosahedral fivefold axes, is the most dominant structural feature among the picornaviruses.

Although similarities in structure and sequence suggest that picornaviruses were derived from a common ancestor, they have evolved to use different cellular receptors for infection. For instance, the human rhinovirus major group viruses use intercellular adhesion molecule-1 (ICAM-1) while poliovirus uses the poliovirus receptor (PVR). These receptors belong to the immunoglobulin (Ig) superfamily and are composed of five and three Ig domains, respectively. Cryo-electron microscopy and image reconstruction analysis has revealed that while ICAM-1 and PVR bind to the canyon region of the virus, they bind in different orientations. Specifically, ICAM-1 stretches deeply into the canyon and interacts with the residues on the canyon floor. Importantly, the residues in the canyon rim region are hypervariable among rhinovirus serotypes, indicating that rhinoviruses mutate the exposed residues as a strategy to escape host immune surveillance. By comparison, PVR interacts with the exposed canyon rim region and partially covers the antigenic epitope of poliovirus. This may partially explain why poliovirus has only three serotypes while the rhinovirus major group has nearly 90 serotypes. A third prototypic picornavirus, echovirus 1, uses $\alpha 2\beta 1$ integrin as its cellular receptor. The binding of echovirus 1 to $\alpha 2\beta 1$ integrin has been mapped to the I-domain, a domain inserted into the $\alpha 2$ subunit. The I-domain, a globular shaped protein, was bound to the exposed canyon region of the virus. Presently, only two serotypes of echovirus are reported to bind to $\alpha 2\beta 1$ integrin. All picornaviruses studied to date recognize the binding receptor by means of complementary electrostatic interactions.

After binding to the specific cell surface receptor, picornaviruses are required to uncoat in order to release the viral genome into the target cell. Two uncoating intermediates of human rhinovirus serotype 3, containing different amounts of RNA, appeared after incubation with ICAM-1 at 37°C. The capsid underwent an expansion step to externalise the peptides, which is account for the density located at the region between the receptor-binding sites and viral fivefold plateau. This increased density could be due to externalized viral peptide. There was no density channel in the capsid but lower density was observed at the canyon region, suggesting the exit of internal components during uncoating.

LIST OF PUBLICATIONS

I. **Xing, L, K. Kato, T Li, N Takeda, T Miyamura, L Hammar, and RH Cheng.** Recombinant hepatitis E capsid protein self-assembles into a dual-domain T=1 particle presenting native virus epitopes. *Virology (1999), **265**, 35-45*.

II. **Xing, L, K Tjarnlund, B Lindqvist, GG Kaplan, D Feigelsto, RH Cheng and J Casanovas.** Distinct cellular receptor interactions in poliovirus and rhinoviruses. *EMBO J.*, (2000), **19**, 1207-1216.

III. **Forsell, K, L Xing, T Kozlovska, RH Cheng, and H Garoff.** Membrane proteins organize a symmetrical virus. *EMBO J. (2000) **19**, 5081-5091*.

IV. **Wu, B, L Hammar, L Xing, S Markarian, J Yan, K Iwasaki, Y Fujiyoshi, T Omura, and RH Cheng.** Phytoreovirus T=1 core plays critical roles in organizing the outer capsid of T=13 quasi-equivalence. *Virology, (2000), **271**, 18-25.*

V. **Haag, L, H Garoff, L Xing, L Hammar, S Kan, and RH Cheng.** Reorganizations of glycoprotein shell mediate alphavirus membrane fusion. *EMBO J, (2002) **21**(17), in press*.

VI. **Xing L, J Casasnovas and RH Cheng** Structures of human rhinovirus complex with intercellular adhesion molecule-1 uncover the dynamics of receptor-mediated virus uncoating. *Submitted*

VII. **Xing L, M Huhtala, V Pietiainen, J Kapyla, J Heino, M Johnson, T Hyypia, and RH Cheng.** The structural basis of integrin action as a virus receptor. *Submitted*

CONTENTS

LIST OF ABBREVIATIONS

AP	Adaptor complexes
CAR	Coxsackievirus-and-adenovirus receptor
CBV	Coxsackievirus B group
Cryo-EM	Cryo-electron microscopy
EV1	Human echovirus - 1
FEG	Field emission gun
FMDV	Foot-and-mouth disease virus
HAV	Human hepatitis A virus
HEV	Human hepatitis E virus
HRV	Human rhinovirus
ICAM-1	Intercellular adhesion molecule - 1
Ig	Immunoglobulin
PFT	Polar Fourier transform
PVR	Poliovirus receptor
STNV	Satellite Tobacco Necrosis virus
SV40	Simian virus 40
T number	Triangulation number
TBSV	Tomato Bushy Stunt virus

1 INTRODUCTION:

1.1 ICOSAHEDRAL STRUCTURE AND QUASI-EQUIVALENCE:

Early in 1956, Crick and Watson concluded that the viral genome did not contain enough genetic information to encode a polypeptide that could encapsidate the whole genome. An example is satellite tobacco necrosis virus (STNV), which is made up of 60 identical 21.5-kD subunits (Liljas et al. 1982). The viral particle has an outer radius of 80Å and an inner radius of 60Å, providing a volume of $9x10^5 Å^3$ for packing RNA. A single hydrated ribonucleotide occupies, on average, 600 to 700 $Å^3$. Thus, theoretically, the STNV virion could only pack a genome of 1200 to 1300 nucleotides in length. Such genome capacity is only enough to encode a protein maximum of 400 residues in size. Crick and Watson suggested that the viral capsid is made up of symmetric array of one or a small numbers of protein molecules. Furthermore, it was thought that cubically arranged arrays would be most practical. The proteins in these symmetrical arrays would have specific bonding properties and would make specific intersubunit contacts that would be repeated in exactly intervals (Crick and Watson 1956). The first experimental evidence for icosahedral symmetry came from the studies of X-ray diffraction characteristics of the tomato bushy stunt virus (TBSV) (Caspar, 1956) and followed by that of turnip yellow mosaic virus (Klug et al. 1957). The investigation of icosahedral symmetry on human rhinovirus 14 and on poliovirus revealed that icosahedral symmetry was a common structural motif among viruses.

An icosahedron contains three type of rotation symmetry, fivefold at each vertex, threefold at the center of each icosahedral face and twofold in the middle of each edge (see the number in Fig 1). A complete icosahedron consists of 60 copies of one type of subunit, where all of the inter-peptide bonds are identical. Indeed, The X-ray crystallographic structure of STNV revealed 60 identical copies of the 25 kDa subunits, no more and no less (Liljas et al. 1982). Each identical subunit is referred to as an asymmetric unit (the grey area in the Fig 1), which is the basic building block of an icosahedral virus.

STNV is a satellite virus, whereby its genome only encodes the structure protein. The replication of STNV needs the "helper virus" tobacco necrosis virus. For simple small RNA viruses, the genome needs the capacity for at lease two proteins, the structure protein (about 1200 nucleotides) and an RNA-dependent RNA polymerase (about 2500 nucleotides). The size of genome requires an icosahedral shell with an inner radius larger than 90Å. Experimental data showed that simple small RNA spherical viruses have outer radii of at least 125Å and the corresponding inner radii of roughly 100Å, which is quite consistent with the size requirement to encapsidate a genome of 3700 nucleotides. Such virus particle

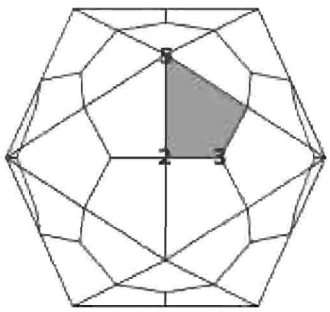

Figure 1: Schematic presentation of icosahedral symmetry. The numbers indicates the positions of the corresponding symmetric axis. One asymmetric unit is marked as grey.

must be formed from more than 60 subunits.

Caspar and Klug derived a general method, the quasi-equivalence, for the construction of icosahedral capsids that contain multiples of 60 subunits (Caspar and Klug, 1962). The basic assumption of the quasi-equivalence theory is that the viral shell is held together by the same type of bonds throughout, but that these bonds may be deformed in slightly different ways in the distinct, non-symmetry related environments. Due to this tolerated flexibility, the viral capsid could include more than one subunit in an asymmetrical unit. Therefore, quasi-equivalence therefore means that the asymmetric unit could be further subdivided into triangles. The T number (Triangulation number) is used to describe the number of triangles in one asymmetric unit and indicates how many types of intersubunit bonds existed in an icosahedral particle. In a T=1 particle, there is only one type of identical intersubunit bond, and total 60 subunits. A T=3 particle has three different environments for the subunits and is composed of 180 subunits. The correlation between T number and the number of different subunit environments is usually maintained. The total number of subunit in a particle always equals to 60T. An icosahedral virus could be said to have a shell of certain T number.

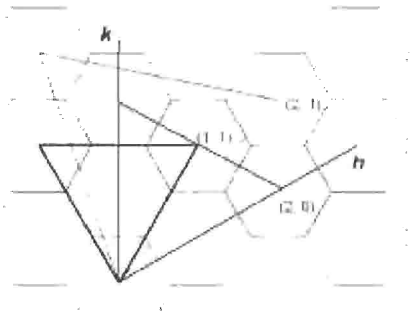

Figure 2: Quasi-equivalence assumes that hexamers and pentamers can be interchanged at a particular position in the surface lattice. The icosahedral shell is generated by inserting 12 pentamers at appropriate positions in the hexamer net. The position at which hexamers are replaced by pentamers are identified by the number of steps along each axial direction required to reach that lattice point (h,k).

A T=1 icosahedral virus could be imagined to have rings of five subunits connected by fivefold symmetry around each of twelve vertices. For capsid made up of multiple of 60, there are six-subunit rings (hexamers) symmetrically inserted between the five-subunits rings (pentamers). An h-k coordinate system is imposed on the icosahedral face with the origin at the first pentamer position. The next pentamer position is identified by the number of steps along each axial direction. The T number can be calculated using the following formula.

$$T = h^2 + hk + k^2$$

The T number could be an infinite series of 1, 3, 4, 7,…, corresponding to 60, 180, 240, 420,… subunits. An example of viruses with different T number can be found in Table 1.

When h is not equal to k, the icosahedral lattice shows different handedness and is said to have a skewed axis. The left-handedness (*l*) refers to the lattice where is h > k, and right-handedness (*d)* where is h < k.

Table 1: Example of viruses with different T number

H	K	T		Example
1	1	3	ssRNA	TBSV
2	0	4	ssRNA	Semliki Forest Virus (SFV)
1	2	7d	ssDNA	SV40
3	1	13l	dsRNA	Rice Dwarf Virus (RDV)
4	0	16	Ds	Herpesvirus
5	0	25	dsDNA	Adenovirus

Viruses utilize the icosahedral symmetry to maximize the genome capacity and to simplify the capsid assembly process. The protein core structure is composed of the folding of the α-helix and β-barrel, which are rather rigid and cannot change in a continuous manner. However, the viral capsid proteins usually contain flexible terminal loops or arms that extend from the core structure. Different orientation of proteins and conformational changes of protein at different quasi-equivalence positions reflect the fact that different intersubunit interactions are made by those flexible loops or arms (Casjens 1997). The structural protein of tomato bushy stunt virus (TBSV) contains a disordered arm region (a) of 35 residues and an internal domain (R) of 66 residues at the N-termini, which are connected to core structure through the hinge region (Hopper and Sauer 1984). TBSV possesses a T=3 icosahedral lattice where the three symmetrically distinct environment are denoted as A, B and C. The proteins at the A, B positions have one hinge configuration and the entire N-terminal region (a and R) is disordered in the crystal structure. The protein at C position, near to the strict icosahedral two-fold, has another hinge position and the connecting arm is folded in an ordered way along the bottom of the S domain (Olson et al. 1983).

To ensure precise assembly, viruses have developed different error-checking mechanisms. One of them is to use different viral proteins to occupy the different quasi-equivalence positions. In picornaviruses, the three similar but not identical proteins locate in an asymmetric unit. Three types of intersubunit contacts are assigned to three different proteins, so that each protein is only engaged only in one type of environment. By this way, viruses reduce the possibility of assembly error that comes from the adjusting the flexible loop structures of the same protein for different environments. This type of icosahedral lattice is called as a pseudo triangulation number instead of true triangulation number. The picornaviruses have a pseudo T=3 (true T=1) surface lattice.

The most striking example comes from simian virus 40 (SV40), where the lattice is formed by 72 pentamers (Liddington et al. 1991). The pentamers also take the hexamer positions and make six different contacts with the neighboring pentamers. The observation that SV40 lattice can be changed from T=7 to T=1 suggested that a nonequivalent subunit interaction is the basic building block to develop T > 1 structures.

1.2 CRYO-ELECTRON MICROSCOPY

1.2.1 Sample preparation:

Sample preparation is the initial steps of structure determination and includes both sample purification and vitrification. Sample purity is key to obtaining high quality data. For these experiments, it was necessary to mix the virus and receptor preparations at a ratio of 1 to 600 (i.e., 10 receptor molecules per binding site on the viral particle), in order to saturate receptor binding. This resulted in a large amount of unbound receptor remaining in solution. The free receptors were then removed from the solution before the plunging step in order to reduce the background. A one ml gel filtration column was used to separate the viral complexes from the free receptors. The fractions containing virus were determined by OD and used immediately to prepare vitrified grids, as described below.

First, virus was frozen onto the supported porous carbon film. Pseudo pores were made of granular glycerol suspended in a Formvar-chloroform solution. Carbon was evaporated on the Formvar film coated grids where the glycerol had been dissolved by methanol. The Formvar was removed by immersing the grid in chloroform. Usually, evaluation by light microscopy was necessary to obtain carbon-coated grids of the correct porosity, in which Formvar had been dissolved without destruction of the carbon film.

The method used to freeze the biological sample was first developed in early 1980's and had been well established (Adrian et al. 1984; Dubochet et al. 1988). Briefly, a 3µl sample solution was applied to the porous carbon grid that has been mounted on a plunging machine. Excess liquid was removed by absorption onto a piece of filter paper. Then, the sample was quickly plunged into a container of liquid ethane cooled in a liquid nitrogen bath. It is critical that the specimen be cooled very quickly so that the water takes on a vitrified form rather than other crystalline forms (which would occur at a slow freezing rate) (Adrian M 1984). It was estimated that the vitrification occurs in approximately 0.1msec. Liquid ethane is preferred over liquid nitrogen because nitrogen has melting point of -196°C, which is too close to its boiling point of -169°C. When the grid is plunged into the cryogen, the surrounding liquid nitrogen is warmed, thereby transforming the liquid nitrogen into gas. This gas layer reduces the temperature transfer rate, so that water turns to crystallized ice instead of vitrified ice. Thus, liquid nitrogen is not a proper cryogen for specimen freezing. The use of ethane, cooled to approximately -170°C, allows formation of a water layer up to 1um thick which is frozen into vitrified ice (Dubochet et al. 1981). While liquid ethane is most commonly used, liquid propane (-186°C and -96°C) can also be used.

In an ideal preparation, the specimen is embedded in a layer of ice that is slightly thicker than the specimen. Obtaining a thin liquid film of the proper thickness on the grid prior to freezing is a crucial step. A commonly used method to form the thin layer of water is to remove excess liquid by blotting rapidly with a piece of filter paper. The blotting time and the humidity of the environment can be used to control the thickness of the water film. A high concentration of virus in the solution is necessary to get ice of the proper thickness.

1.2.2 Data collection:

The vitrified or frozen-hydrated virus sample was then transferred into the electron microscope and was observed at the ice-embedded state. A cryo-transferring system was used to maintain the specimen at or lower than -160°C during the transfer steps and in the microscope in order to avoid devitrification of the sample (Adrian et al. 1984). The grid was mounted onto a cryo-holder in a cryo-workstation. The cryo-workstation keeps the holder secure during sample cool-down and sample loading before transfer of the holder into the microscope. Unlike other traditional EM holders, where just the specimen cradle is cooled, the entire tip of the cryo-holder is cooled. As a result, temperature gradients around the specimen are small, drift is minimal and specimen temperature is stable and easily monitored.

In the microscope, it is crucial to keep the electron dose as low as possible. Any interaction of electrons with the biological sample will alter the structure. This low dose mode is particularly important to prevent exposure of the area of interest. The specimen is firstly viewed at low magnification (e.g., 2650X using a Philips CM120 transmission microscope) to find suitable areas in which high concentrations of particles are uniformly distributed in single layers. Once a suitable area is found, focusing at high magnification is done adjacent to the area of interest (e.g., 3 um away in the case of magnification at 45kx). The micrographs presented in this thesis are recorded at a magnification of 45,000x at an electron dose of approximately $10e^{-}/Å^{2}$.

Without heavy metal staining, frozen-hydrated specimens have very low contrast. Therefore, it is necessary to defocus the microscope's objective lens in order to improve the contrast (Adrian et al., 1984). The image is nearly always underfocused, so that the information from the specimen is negatively transferred onto the image before the first contrast transfer function (CTF) zero.

1.2.3 Image formation and Contrast transfer function:

Essential components of a transmission electron microscope include electron source, the gun, and condenser lenses that direct the electrons through the specimen at the desired angle and over the appropriate range; the objective lenses and additional lenses; and a detection system for viewing (fluorescence screen), recording (photographic film) and analysis (energy filter etc).

In the transmission electron microscope, the condensers are programmed to provide a parallel beam of electrons through the specimen. In the case of a biological sample, where almost all the incident electrons pass thought the object, a small fraction will be scattered by the specimen. Among the scattered electrons, some have lost some energy (inelastic scattering) and others have changed direction without energy loss (elastic scattering). The information about specimen structure is expressed as the angular distribution of the scattered electrons and recorded as the contrast in the image. The contrast is created by two mechanisms: the scattering contrast (amplitude contrast) and the phase contrast. The phase contrast is generated by the interference of the scattered electron wave that passes through the objective aperture with the unscattered electron wave. The amplitude contrast is produced by the loss of electrons that are scattered outside the objective aperture.

The amplitude is a measure of electron current distribution at any plane in the microscope and hence, determines the image (Hawkes, 1991). The phase describes the direction in which the electron is traveling. Therefore, it is lost on the image, because the image records the detected electrons, but is insensitive to the direction from which they came. In an unstained vitrified sample, there are many more electrons scattered elastically than inelastically and mainly unscattered and elastically scattered electrons are involved in contrast formation. Therefore, the information about a specimen that is conveyed by the beam is due to the image contrast that consists mainly of the phase contrast.

The Fourier transform of a phase-contrast image $T^{i}_{ph}(\alpha,\varphi)$, is directly proportional to the object transform $T^{o}(\alpha,\varphi)$ which is described by the expression (Erickson and Klug 1971):

$$T^{i}_{ph}(\alpha,\varphi) = - T^{o}(\alpha,\varphi) \sin \chi(\alpha) \quad (1)$$

Where a can be identified physically as the angle of scattering in the microscope, and φ is the azimuthal coordinate. The minus sign indicates a reduction in electron intensity over areas of high mass density, the condition of normal contrast. The term ?(a) refers to the phase shift, where the scattered electron wave undergoes at the diffraction plane of the microscope. In the image formation theory, the effects of spherical aberration (*Cs*) and defocusing (*Df*) are attributed to a phase shift, where:

$$\chi(\alpha) = 2\pi/\lambda \, [-Cs\alpha^4/4 + \Delta f\alpha^2/2] \quad (2)$$

The Fourier transform of a amplitude-contrast image $T^{i}_{am}(\alpha,\varphi)$, is given by an expression that similar to equation (1):

$$T^{i}_{am}(\alpha,\varphi) = - T^{o}(\alpha,\varphi) \, Q(\alpha) \cos \chi(\alpha) \quad (3)$$

Amplitude-contrast is defined in the theoretical derivation as that due to the real part of the scattered wave. Phase contrast, for which the transform function is proportional to sin ?(a), is defined with the imaginary part. *Q*(a) gives the magnitude of the real part of the scattered wave relative to that of the imaginary part, i.e., the ratio of amplitude contrast to phase contrast. In general amplitude contrast and phase contrast are both contributed, independently, to the image, and the total image transform can be written as:

$$T^{i}_{total}(\alpha,\varphi) = - T^{o}(\alpha,\varphi) \, [\sin \chi(\alpha) + Q(\alpha) \cos \chi(\alpha)] \quad (4)$$

Alternatively, the contrast transfer function [sin ?(a) + *Q*(a) cos ?(a)] could be written as sin [?*(a)* + *F (a)*]. This useful transformation shows that the effect of a small fraction of amplitude contrast can be treated as an additional phase shift, *F (a)*, in the phase contrast transfer function. The resulting image will be a faithful representation of the structure only if a number of important conditions regarding both specimen and microscope are satisfied. First, both the size of the electron source and the energy spread of the beam electrons must be very small for reasons of coherence. If the source is not small, the beam incident on the specimen will not be parallel, traveling along the optical axis, but will contain electrons traveling in slightly different

directions. The interference fringes that form the images are quite sensitive to the direction of incidence of electrons on the specimen and will be blurred if a range of directions is present. If the source emits electrons with more than a narrow energy range, the phase difference between the unscattered and scattered electrons will result in spreading and the interference fringes will be blurred.

In practice, the incident electron beam is only partially coherent, i.e. the indicating waves on the specimen vary in both direction and wavelength (?). The variation in the beam direction leads to so-called 'partially lateral coherence' and the variation in wavelength leads to so-called 'partially temporal coherence'. The illumination aperture (Zemlin 1994) generates partially lateral coherence. The influence of partially lateral coherence on the phase-contrast image is to dampen the high spatial frequencies in the phase contrast function, i.e. to reduce the resolution. In principle, it is always possible to increase the lateral coherence arbitrarily by reducing the magnification of the illuminating source. But increasing the coherence in this way leads to a decrease of the beam density. A very low beam density, in turn, requires extremely long exposure times. The high coherence of field emission gun (FEG), due to its high brightness and small source size, is recognized as an important advantage over the thermionic source. A higher coherence with sufficiently strong beam density can be achieved with an FEG due to its 1000X higher brightness as compared to a thermionic electron source (Zemlin 1994). The effect of the energy spread is to impose an envelope function on the phase contrast function in order to weaken the transferred signal toward a high spatial frequency. Monochromicity of beam would be optimal for the constructive interference used in phase contrast imaging. By using FEG, the fading to high frequency appears to be significantly weak compared to that with a thermionic source. This is a very valuable advantage since the contrast of the biological structure by itself is very weak. Besides the high coherence, the small source size of FEG makes the spot-scanning technique possible. During the exposure of a radiation-sensitive biologic sample, the movement that occurs in the specimen

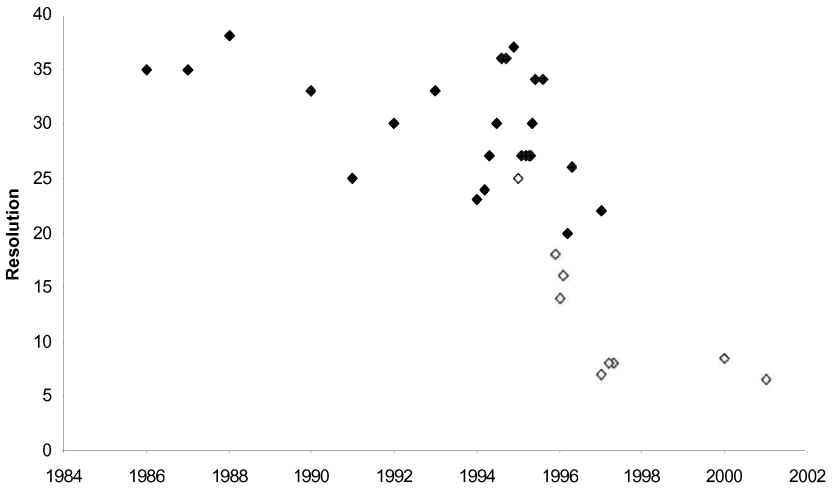

Figure 3: The improvement in the resolution of published icosahedral reconstruction from cryo-electron micrographs (modified from Mancini et al. 1997).

blurs the image and reduces the resolution. Scanning the specimen with a very small spot beam could minimize the effect of this movement (slow scan CCD technique). The intermittent non-radiated margins of such small spots act like a stabilizing buffer. The significance of using FEG to enhance the resolution in the study of biological samples is illustrated in Fig 3.

1.2.4 The three-dimensional reconstruction:

Since the specimen projection is recorded on SO163 film, the projection density s (x, y) of the specimen is thus proportional to the logarithm of the optical density of the electron micrograph (Crowther 1971). In order to perform image processing, such as Fourier transformation, the electron micrograph is first scanned with a computer-controlled film scanner, which provides a digitized image of the optical density distribution of any selected area. All further operations, such as Fourier transform, and compilation of different views then can be performed with a computer. The notable difference to X-ray crystallography, which lacks phase information from the measurement, is that both amplitudes and phases of the Fourier transform can be obtained directly from the image. This is because the complex Fourier transform is generated by computation from the array of digitized optical densities representing the image.

The use of image processing assumes that all the individual virions have an identical structure and are randomly oriented in the electron microscope. The EM image of an icosahedral particle approximates a two dimensional projection of its structure. The Fourier transform of this projection is a section plane of its three-dimensional Fourier transform; the section is normal to the view direction and passes through the centre of a 3D transform (central section) (Crowther 1971). Once the orientation of these particles is established, the images of separate particles in different orientations are merged together. Then, the three-dimensional reconstruction is produced by Fourier inversion. Therefore, the central task in the three-dimensional reconstruction is to determine the orientation of each individual particle.

The orientation defines the position of the viral particles in the vitrified ice relative to the incident electron beam, or which angle a particle is projected. The orientation of a particle is described using three angular parameters (θ, φ, ω) in Z-Y-Z' rotation order (Fig 4). Angle q defines the rotation around the Z-axis (X-, Y-, and Z-axis are three vertically intersected twofold axes). Angle j defines the rotation around the Y-axis and angle w defines the rotation around the newly generated Z-axis. An asymmetric unit of an icosahedral particle includes the region of angle θ from 69^o to 90^o, of angle φ from -32^o to 32^o, and of angle ω from 0^o to 360^o. Two methods are commonly used to determine the angular parameters: the common lines method and the Polar Fourier Transformation (PFT).

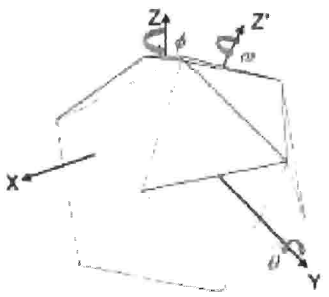

Figure 4: T=1 icosahedron and the definition of orientation in Z-Y-Z rotation order.

1.2.5 Common lines:

The common lines method (Crowther 1971) was the first Fourier method described for determining the orientation of an icosahedral particle. The common lines are related to the symmetry of the object and arise when the symmetry axis is not along the projected direction. Assuming a particle has one threefold rotational symmetry, the Fourier transform of the projection possesses the same symmetry as the original particle, with the same orientation of the symmetry axis. All the points in the original section (A) have an identical copy in a new section plane (B), which is derived from the original section by a 120^{o} rotation about the threefold axis. These two sections intersect at a line called AB. In the same way, another line results from the intersection of plane A and plane C that is a 240^{o} rotation from the original section. Along these two lines, the transforms have identical values for each of the corresponding points moving along the lines. These two copies of a line are called "common lines" in the original transform section.

Each symmetry operation and its reverse about an axis generate a pair of common lines, which lie to either side of the view axis. Two pairs of common lines were generated from one fivefold symmetry. A threefold axis generates one pair, and a twofold axis generates one real line (Friedel symmetry). An icosahedron contains six fivefold axes, ten threefold axes and fifteen twofold axes, giving rise to a total of 37 pairs of common lines (self common lines). The common lines are well separated in an orientation nearest to the centre of an asymmetric unit. When the icosahedron is viewed along or near to the symmetrical axis, certain common lines will overlap with each other, resulting in a reduced number of independent common lines.

The orientation of common lines depends on the direction of projection with respect to the symmetry axis. Therefore, if the position of the common lines was defined in the transform section, one could deduce the orientation of the particle with respect to its symmetry axis. For each trial viewing direction, the position of the common lines can be calculated, and the values of the observed transform compared at corresponding points. An error-function is calculated and has its minimum value when the trial orientation coincides with the one actually used. "Phase residual" is generally used as the error-function. The simplest form of orientation search is then the calculation of the sum of phase residues between 37 pairs of common lines in 1^{o} steps for each of the orientations in the asymmetric unit (*emicofv*). So the program first fixes the degree of the ϕ angle for a theta angle, and then calculates the phase residues for every omega angle. However, while determining the orientation, it also is necessary to locate the particle centre, with the assumption that the centre of the transform lays at the centre of symmetry of the icosahedron. After initial searching, the position of the centre can be refined by small adjustments in order to minimize the common lines residual for that orientation.

Another application of the common lines method comes from the comparison of transforms of two different particles (*emicograd*). Once the orientations of the projections of these two particles have been determined, the position of common lines between the two projections can be calculated. By rotating one of them about the symmetry axis, 59 other intersections can be generated (one for each symmetry element). This gives 60 pairs of lines that have the common value in two transforms, since they were derived from the same structure. The sum of the phase residual indicates the difference in degrees when the orientation of the second particle is

compared to that of the first one. This is especially useful for determining the consistent hand for the particles. The projection from a particle oriented from (θ, φ, ω) (un-flipped) is indistinguishable from (θ, φ, ω+π) (flipped). They have identical phase residuals in self-common lines but differ in cross-common lines when they are compared with the third particle of fixed orientation. The proper hand for such a structure must be selected by trying all the possible combinations of un-flipped and flipped particles for the entire data set.

1.2.6 Polar Fourier Transform:

Polar Fourier Transform (PFT) is a model-based orientation-determining program (*empft*) (Baker and Cheng 1996). It uses a cross-correlation procedure to compare raw images with a series of reference projection views produced from a 3D density model. The model could be a 3D density map or a computed icosahedral object, for example, from an atomic X-ray crystallographic structure.

The reference projection views were first generated by back-projecting a 3D model map according to defined orientations. Two program files were written and used for later comparison with the raw image. Projection of the model in 1^{o} angular increments for orientations encompassing half of an asymmetric unit (θ from 69^{o} to 90^{o}, φ from 0^{o} to 32^{o}) (*pft.prjs*) could result in as many as 382 separate views. The projection views are then interpolated onto a 2D polar grid with axes of r (radius) and ? (azimuthal angle) according to their respective centers. A 1D Fourier Transform was obtained from the polar data at each radial row (*pft.pfts*) and displayed with axes of r (radius) and G (reciprocal of ?). The spectra distribution is related to the periodic repeats in each row of 2D polar projection.

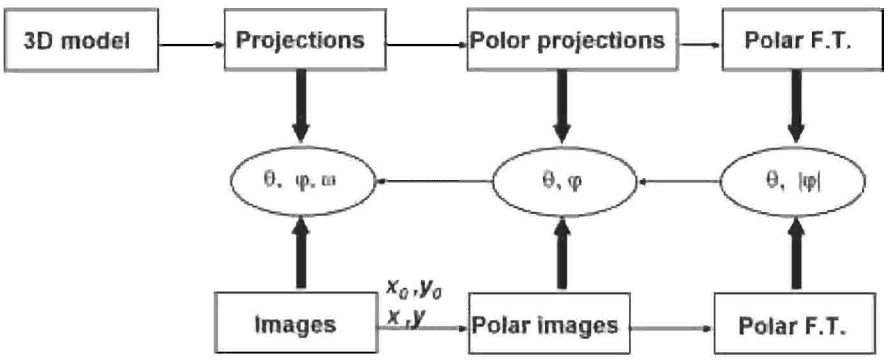

Figure 5: The flowchart of polar Fourier transform program. A series of projections are computed from the 3D model and are used to estimate the initial center of the images (x_0, y_0). Then the polar interpolation and polar Fourier transform were calculated on the data based one the center of (x_0, y_0) and on the 3D model. The correlations of the polar Fourier transform between data and model projections give the angular parameters of (*?, |f |*). The sign of *f* angle of each image is obtained with correlation between polar image and polar projection. The angular parameter of ? is determined by the correlations of image and projections. Then the center of each image (*x, y*) is refined with correlation of image with (?,f ,?) corresponding projection. The refinement of angular parameters was done with the same procedure.

The centre of each image has to be obtained in order to resample the raw data onto polar grid (Fig 5). The parameter,(x_0, y_0), was first assigned by the cross correlation of the images against a circular reference. The circular reference was generated by circularly averaging the projections, which involves summation of the projection views. The polar images were then obtained by interpolation of the raw data according to the centre (x_0, y_0) and thus the polar Fourier transform of these images. Cross-correlation between image files and reference projections was introduced to assign the polar angles. Angles θ and |φ| were given by the correlation between the polar Fourier transforms. The comparison of these polar projections with polar images gives the sin of angle φ. Angle ω was obtained from the comparison of projections with images based on the known θ and φ angles (Fig 5). After discerning the values for angles θ, φ and ω, the image was then compared with the projection of (θ, φ, ω) to refine its centre (x, y). The orientation of this image will be redefined with the same procedure based upon the new centre (x, y).

The common-lines method and the PFT method are the two most commonly used orientation determination methods in the field. Both of them use the information in the reciprocal space. However, the common lines method is directly related to the icosahedral symmetry where only the information on the 60 pairs of common-lines is obtained. In contrast, PFT relies on a noise-free model to screen the images and to refine the orientation of individual images. PFT, compared to the common lines method, uses all the available information in both Fourier space as well as real space. Moreover, PFT is not related to icosahedral symmetry and can be used to refine the image of an object without any symmetry.

1.2.7 The importance of centre determination and rHEV paper:

The combination of common lines and PFT methods was used in our procedure to resolve the 3D structure of viruses. For example, recombinant hepatitis E virus (rHEV) (paper I) was self-assembled with a truncated virus ORF2 structural protein, which was expressed in insect cells using a recombinant Baculovirus system. The

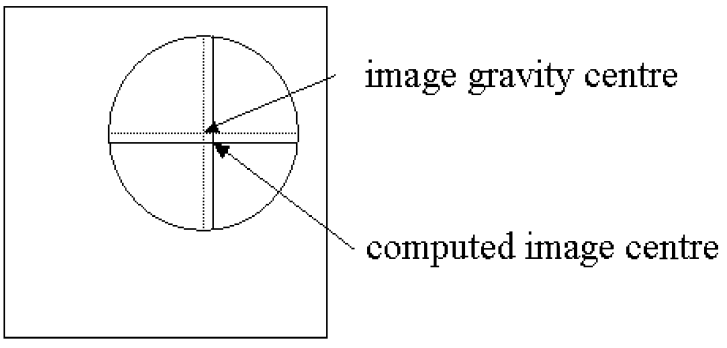

Figure 6: The schematic drawing of algorithm in center determination. The gravity center of a spherical image should be superimposed on the particle projection center. The errors may be caused by the particle distortion or the contrast gradient due to the thickness of the ice.

cryo-electron micrograph showed less density in the centre of the capsid indicating that the capsid of the rHEV particle was empty. The particles appeared as spherical shapes in the central ring and had a spike-like density. For image processing, a standard correlation coefficient method was first used to determine the image centre of each individual particle. Therefore, the centre (*x, y*) of each individual image was estimated by cross-correlation of the image to an average image summed from the entire data set (*emcororg*). With this data, the angular parameters (θ, φ, ω) were estimated by the self-common lines method. A 3D density map was reconstructed from the selected images based on their estimated orientation and was used as a first model for PFT refinement. However, a stable reconstruction could not be obtained using this method. In reviewing the five parameters (θ, φ, ω, *x, y*) of the individual images during each run, it was determined that the parameters were not constant. This may be due to the fact that the centre of the rHEV image is difficult to lock because of its lower density in the central region of the particle projection. The 2D transform of an electron image is comprised of a central section passing through the 3D transform of the specimen. Therefore, defining the centre is of particular importance because all of the common lines intersect each other at this point and because the polar image is generated by using this point as the origin of the radius. Any aberrance in locating the centre will be emphasized by inaccurately determined angular parameters. To improve the precision of centre determination, an additional criterion was introduced: the gravity centre of each image (Fig 6). Because icosahedral symmetry is imposed by the viral particle, the gravity centre of each spherical image should be the same as the centre of the projection. The distance between the gravity centre and the centre calculated by cross correlation indicates the precision of the centre determination. If the distance is larger than a predetermined threshold, the image is reset using the gravity centre. Finally, the reconstruction of the rHEV particle was accurate to the resolution of 25Å, as indicated by the R-factor.

1.2.8 Map reconstruction:

With determined angular and central parameters, image data then is merged in Fourier space, and a Fourier inversion is performed to generate a 3D map in real space. A density map then can be expanded using the cylinder function:

$$? (r, f\ z) = ?\ \ ?g_n (r, Z) \exp (inf) \exp (2p\ I\ zZ)\ dZ \qquad (5)$$

the Fourier transform is then expressible in the form of

$$F(R, F, Z) = ?\ Gn\ (R, Z) \exp (in\ (F\ + ½\ p)) \qquad (6)$$

where *Gn (R, Z)* is the Fourier-Bessel transform of g_n *(r, Z):*

$$Gn\ (R, Z) = ⅋_0^{8}\ g_n\ (r, Z)\ J_n\ (2pRr) 2pr\ dr \qquad (7)$$

and conversely,

$$g_n = ⅋_0^{8}\ Gn\ (R, Z)\ J_n\ (2pRr) 2pR\ dR. \qquad (8)$$

The equation (2) states that for fixed R and Z, which are around an annulus normal to the polar axis, the transform *F* is a known function of *F*, independent of the particular density ？. The *Gn (R, Z)* represents the coefficients in a one-dimensional Fourier analysis of the transform around the annulus. If the observed transform values *F* are located at equally spaced points around the annulus, the *Gn (R, Z)* can be calculated by inversion of *F* with equation (2). Then, g_n can be obtained from equation (4) and thus the density ？ from equation (1). The method also is valid if the sampling is not in regular form. In that case, *F* will be located at every point where an observed transform plane cuts the annulus. Assuming there are at least as many observed data points as unknown *Gn* on the annulus, equation (2) can be regarded as observational and can be solved for *Gn* using the least squares method.

Knowledge of any symmetry that a particle possesses is useful for reducing the size of the least squares problem. For cylindrical coordinates, the polar axis may be superimposed on top of one of the symmetry axes with no restriction on the order of the symmetry axes. This results in reduction of the number of *Gn*'s, since only those indices that are integral multiples of the rotation symmetry need be included. Clearly, the symmetry axis of the highest order should be chosen as the polar axis. Since it also is possible to explicitly include twofold axes at right angles to the rotation axis chosen as polar axis, all the cyclic and dihedral symmetries can be fully expressed as cylindrical coordinates. However, an icosahedral group of 532 cannot be fully accommodated. Instead, the dihedral group 522 is used for cylindrical coordinates in this case.

A single view of the particle gives a number of central sections of the transform, related by the appropriate rotational symmetry operations. For example, a general view of an icosahedral particle provides 59 other symmetry-related views and the three-dimensional transform can be filled in accordingly. If the direction of view is a special one, such as along the symmetry axis, the number of unique views will be smaller.

Map reconstruction is the last step of image processing and is carried out using several computing programs. The first program (*emicomat*) applies symmetry to the Fourier transform of each particle, resulting in 60 sections out of each particle in the 3D Fourier space. The Fourier terms of all these sections are extracted and are arranged into a normal matrix that is set up for each annulus in the polar coordinates. The second program (*emicobg*) combines the normal matrix from a number of different images and solves them to give *Gn*'s. g_n is generated by summing up the Bessel functions of different orders (*emicolg*). And finally, a 3D map was generated by integrating g_n. (*emicofb*) in the "standard" 2-fold setting.

1.2.9 Map interpretation:

The structures of both picornaviruses and most of their cellular receptors have been resolved to the atomic level using x-ray crystallography. This information is helpful for interpretation of the reconstruction of receptor-bound viruses. The coordinates of both the viral protein and receptor could suggest docking as determined by the corresponding density and the detail contacts at the molecular interface, which can be revealed at reasonably high resolution. Program O was used to fit the atomic structure

into a cryo-EM map. The cryo-EM density cannot directly be downloaded into program O until the data is reformatted into a dn6 density map. Differing to cryo-EM convention, program O uses the positive density map instead of the negative density map. Due to the large differences in resolution between the cryo-EM map and the coordinates, a register is usually needed during the fitting. This register can be a defined terminus of the peptide chain, the sugar density etc.

The difference map, representing the receptor density, was generated by subtraction of the viral capsid density from the receptor-virus complex map. The capsid density was computed from X-ray atomic coordinates using the XPLOR program. The coordinates then were used to calculate a set of structure factors from which an electron density map was generated at a resolution corresponding to the EM density (Cheng et al. 1994). The procedure can be divided roughly into four steps, editing of the pdb file, building of the molecular structure, computing the structure factor, and calculating the density map (Belnap et al. 1999). First, downloaded coordinates must be edited with the program *deal_pdb*. This includes: 1) removes the header and any lines except "END"; 2) deletes the coordinates of water and heavy atoms; 3) changes the names of strange atoms, , for example, OXT to O; 4) renumbers the atom starting with 1; 5) removes the chain ID; and 6) as the line immediately preceding the "END", adds an extra oxygen atom labeled with OT at coordinates slightly different than the previous oxygen Secondly, the molecular structure is built using the XPLOR program (Brunger 1992). Three XPLOR files, *tophcsdx.pro, parhcsdx.pro, and toph19.pep*, are needed for adding the hydrogen atoms. Toph19.pep includes the information about the peptide-bond linkage. The files tophcsdx.pro and parhcsdx.pro contain the information about polar hydrogens in order to obtain hydrogen-bond potentials. The next step is to calculate the structure factor using the XPLOR program. In this step, one has to set the unit cell value to a chosen value large enough to encompass a viral particle, and set the resolution compatible with the cryo-EM density map. Finally, the density map based on the calculated structure factor is generated.

The difference map was loaded into O program. The coordinates of the corresponding receptor were read and manually docked into the density using the command of *move_zone*. The docking was then optimized to minimize the side-chain crashes made by receptor residues and the viral surface residues. The resulting model was used to calculate a set of structure factors from which an electron density map was thus generated at a resolution corresponding to the EM density. The real-space correlation between the calculated and the experimental densities was computed, where the high value of the correlation coefficient indicated optimal positioning of the receptor molecule.

1.3 PICORNAVIRUSES AND ITS CELL ENTRY

Picornaviridae comprises many important human and agricultural pathogens, such as human rhinoviruses (HRVs), poliovirus, foot-and-mouth-disease virus (FMDV), and human hepatitis A virus (HAV), (Table 2). Because of their medical and economic importance, it is not surprising that picornaviruses have played a central role in the development of modern virology. For example, the studies discovery that poliovirus could be propagated in cultured cell (Enders et al.1949) ushered studies on molecular

requires viral protease 3CD and the completed correct folding of P1 protein. The heterotrimers then assemble into pentamers (14S) and the pentamers can further associate into empty capsids in the absence of RNA. It is not yet known whether the RNA is encapsidated into the empty capsids or whether it nucleates the pentamers. The maturation cleavage of VP0 into VP4 and VP2 occurs after RNA packaging and significantly increase the virion stability by forming of a number of intra-protomer and intra-pentamer interactions. This completion of the internal network finalizes the assembly process and makes the assembly irreversible. An RNA-containing virion with VP0 lacks infectivity until the maturation cleavage takes place.

Table 3: Comparative summary of VP1 N-terminal and VP4 structures

	HRV3	HRV14	HRV16	HRV 1A	HRV2	Polio 1	Polio 3
	antiviral group A		antiviral group B				
Number of amino acid in VP1	288	289	285	287	289	302	302
Visible VP1 region in crystal structure	1016-1283	1014 -1289	1001-1285	1005-1287	1007-1009, 1015-1283	1006-1010 1020-1302	1007-1010 1024-1302
Confirmation of VP1 N-terminus	disordered	disordered	1001-1012 an a-helix	1005-1012 an a-helix	1007-1009 ß-strand	1006-1010, ß-strand	1007-1010 ß-strand
Residual number of VP4	68	68	68	68	68	68	68
Visible VP4 region in crystal structure	4029-4068	4026-4068	4001-4007, 4023-4044	4026-4044	4002-4006, 4024-4043	4002-4016, 4023-4068	4002-4016, 4027-4030
Confirmation of VP4 N-terminus	disordered	disordered	4001-4007 4023-4038 antiparallel ß-strands	disordered	4002-4006, 4024-4030 antiparallel ß-strands	4003-4006 4027-4030 antiparallel ß-strands	4003-4006 4027-4030 antiparallel ß-strands
Myristate on VP4	disordered	disordered	ordered	ordered	disordered	ordered	ordered
RNA	stacking against 2038	stacking against 2038	stacking against 2038	None identified	stacking against 2038	stacking against 2038	stacking against 2038
Citation	Zhao et al., 1996	Arnold &Rossmann, 1985	Hadfield et al., 1997	Kim et al., 1989	Verdaguer et al., 2000	Hogle et al., 1985	Filman et al., 1989

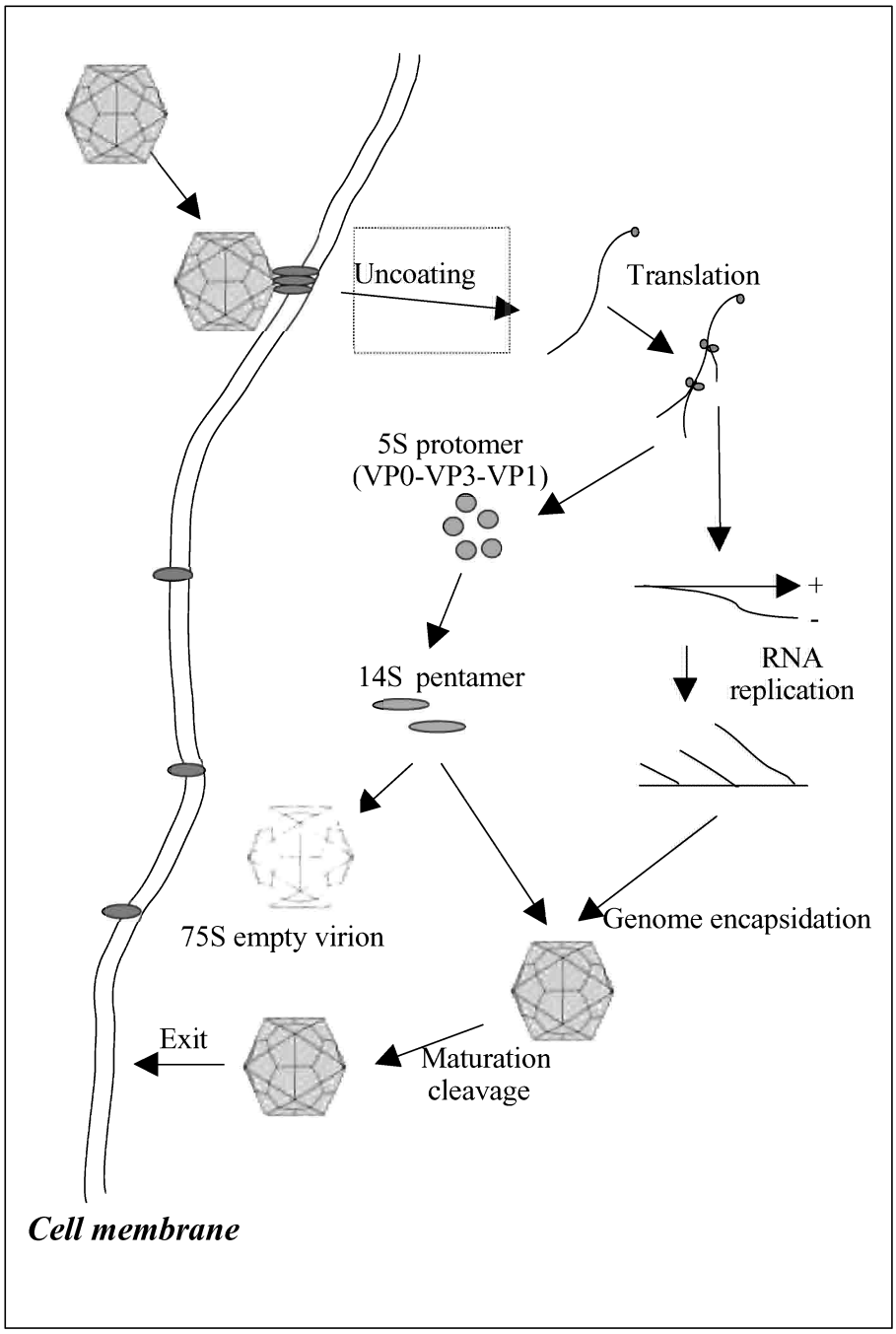

Figure 10: Schematic presentation of picornavirus life cycle.

1.3.3 Attachment of virus to its cellular receptors on the cell surface

All the picornaviruses require cellular surface proteins as receptors for their cell entry. The cellular receptors identified for different picornaviruses are listed in the

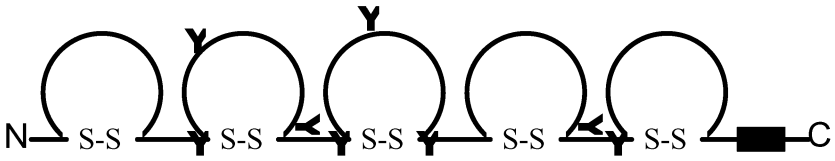

HRV major group receptor (ICAM-1)

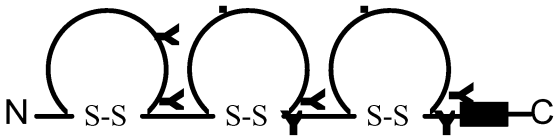

Poliovirus receptor (PVR)

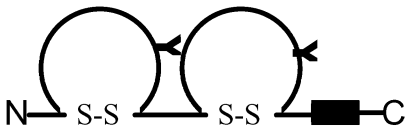

Coxsackievirus and Adenovirus receptor

Figure 11: The diagram presentation of immunoglobulin receptors. The black box indicates the transmembrane region, which does not existed in the soluble receptor form. The potential sugar position is marked as Y. S-S indicates the potential position of disulfide-bridge.

The first step in viral infection is the attachment of the virion to its specific receptor on the cell surface. The earliest clues that picornaviruses do not use the same receptors were based on differences in the susceptibility of their receptors to digestive enzymes (Colonno et al. 1986). For example, poliovirus and rhinovirus receptors were destroyed by trypsin, while the receptor for Coxsackievirus B group was inactivated by chymotrypsin. The virus-receptor interaction is an important determinant of cell tropism, which often correlates with host specificity, and the symptoms of viral disease.

The picornavirus receptors include a variety of cellular membrane proteins. These proteins have their normal physiological functions and their natural ligands. Intercellular adhesion molecule–1 (ICAM-1), poliovirus receptor (PVR), and coxsackievirus and adenovirus receptor (CAR) belong to immunoglobulin (Ig) superfamily and consist of five, three and two Ig domains, respectively (Fig 11). In these receptor molecules, mutational analysis demonstrates that the virus-binding

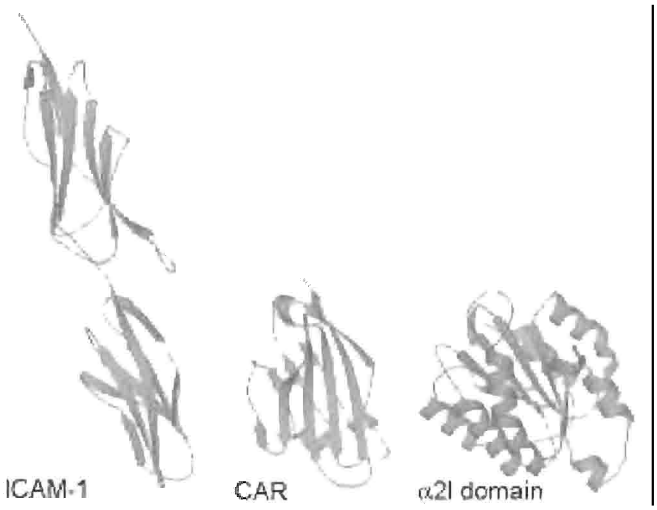

Figure 12: The atomic structures of picornavirus receptors. Two and one N-terminal immunoglobulin domains have been solved with X-ray crystallography on ICAM-1 and CAR receptor, respectively and are formed mainly with b-barrels (Casasnovas, 1998), (van Raaij MJ, 2000). The inserted domain on α2 subunit of α2β1 integrin contains central b-barrels surrounded by a-helices (Emsley, 1997).

region is in domain 1 (Ig domains are numbered from the N-termini). The N-terminal first two domains of ICAM-1 and the N-terminal domain of CAR were successfully crystallized and the structure has been solved (Casasnovas et al., 1998). Domain 1 of ICAM-1 belongs to I set of IgSF domains and contains β-sheets running parallel or antiparallel to the long axis of the domain (Fig 12). A disulfide bond covalently links FG- and BC-loop on the tip of domain 1. There are four residues serving as hinge between domain 1 and domain 2. Residue Trp84 has two main chain hydrogen bonds to Ala114 in BC loop of domain 2. The FG-loop of domain 2 extends the furthest towards domain 1 and makes the most contact with domain 1, which rigid the angle between domain1 and domain 2. ICAM-1 was found as homodimer in crystal structure. The dimeric contacts involve hydrophobic residues at DE-loop of domain 1. FMDV and some of human enteroviruses are found to utilize integrin molecules as their cellular receptors. Unlike Ig molecule, integrin is heterodimer of α and β subunits. The structure of extracellular region of integrin αvβ3, the receptor of FDMV, has been solved with x-ray crystallography (Xiong et al., 2001). The N-terminal segments of α and β subunits assemble into ovoid "head" from which two nearly parallel "tails" emerge. The head consists of a seven-braded β-propeller from αV subunit and an βA domain looping out from a unique Ig-like "hybrid" domain in β3. However, the collagen-binding integrin, α2β1 integrin, have A-domain (I-domain) inserted in α2 subunit (αI domain), which is responsible for ligand recognition. Attempts have been made on the structural study of α2I domains. Like βA-domain, α2I-domain has a central six strands of β-sheet surrounded by eight α-helices (Fig 12) (Emsley et al., 1997). A metal-ion-dependent-adhesion site (MIDAS) motif was found to occupy the crevice at top of the central β-strand. Mg^{++} ion is

needed to maintain the collagen binding function of α2I-domain.

Table 4: Picornaviruses and their receptors

Virus	Serotypes	Receptor and Description
Human rhinovirus (major group)	91	ICAM-1 (intracellular adhesion molecule 1, CD54), Immunoglobulin molecule, 5 domains 1, 13, 32
Human rhinovirus (minor group)	10	LDLR (low density lipoprotein receptor) 1, 17
Poliovirus	3	Poliovirus receptor (CD155) (Immunoglobulin molecule, domains)
Coxsackievirus A13, A18, A21, Coxsackievirus A9,		ICAM-1
Echovirus 22		$\alpha_v\beta_3$ integrin
Echovirus 1,		VLA-2 ($\alpha_2\beta_1$ integrin)
Echovirus 6, 7, 12		DAF (decay accelerating factor, CD55)
FMDV	7	$\alpha_v\beta_3$ integrin

Cryo-electron microscopy has been proved as one of the most powerful tools to study biological dynamic events. The quick freezing technique captures the sample in its nearly native condition. Image reconstruction provides a density profile that can be fitted with the atomic coordinates of each interacting component if these have been determined by X-ray crystallography or NMR, and thus the molecular interface can be defined at a reasonable precision. Such combination techniques have been widely used in determining biological movement, such as muscle contraction, ion channel opening, and interaction of viruses with antibodies and/or receptors. This combination method was first demonstrated in 1993 in investigation of the interaction of HRV16 with a soluble form of its receptor, the two-domain fragment of ICAM-1. The complex was prepared by incubation of ICAM-1 with HRV16. The three-dimensional reconstruction revealed that the viral capsid was saturated with 60 copies of receptor (Olson et al., 1993). This is in consistence with the biochemistry experimental result that suggested that receptor-virus binding in one to one ratio (receptor vs binding site) (Hoover-Litty and Greve 1993). ICAM-1 has an approximate dumbbell shape, which is consistent with a two-domain structure. The position of ICAM-1 showed that it bound to the canyon as predicted by the canyon hypothesis. Since the structure of ICAM-1 was not available at that time, the fitting was done with coordinates of CD4, a molecule highly homologous to ICAM-1. The molecule makes contact with south wall of the canyon and its tip could reach the canyon floor. Correlation of the solved structure with the mutagenesis data provided an unambiguous view of receptor binding.

1.3.4 Entry of picornavirus into host cells

After attachment to the receptor on the cell surface, the picornavirus genome has to gain access to cellular translation machinery, which is compartmentalized in the cell cytoplasm. The best way for a positive stranded RNA virus to release its genome is to uncoat the capsid at an environment most close to the cytosol, i.e. at the cellular membrane or, in most cases, in the endosome. The clathrin-mediated pathway is the most well documented endocytosis process. Clathrin coats are involved in the transportation of molecules from the plasma membrane to the early endosomes, forming pits that invaginate to become free clathrin vesicles (Marsh and McMahon 1999). The proteins called clathrin heavy chain and clathrin light chain are the main components of these coats. They are associated with each other and can form complexes of three-legs trimer, the triskelions, which can assembles into polygonal arrays both in vitro and in vivo. Other component includes the adaptor complexes (APs). APs can interact with membrane proteins that contain appropriate signals for sorting into clathrin-coated vesicles, linking clathrin to the membrane; and therefore to promote the formation of clathrin coated vesicles. So far, four types of endocytic sorting signals have been identified, i) tyrosine (Y) based signals in the form FxNPxY or YxxØ (Ø is a large hydrophobic residue), ii) dileucine-containing signal, iii) phosphorylated serine-rich domains, iv) motifs involving ligand-induced phosphorylation of serine residue and the ubiquitination machinery (Marsh and McMahon 1999).

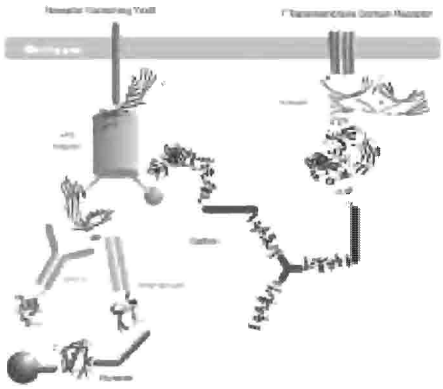

Figure 13: Atomic structures of domains of proteins that involved in clathrin-dependent endocytosis (Marsh and McMahon, 1999)

The receptor on the cell surface serves as the target for virus attachment, and the binding of virus to the receptor can be the signal to trigger virus internalization. De Tulleo and Kirchhausen showed, with indirect immunofluorescence, that the infection of HRV14 (a member of major rhinovirus major group) was blocked by inhibition of clathrin dependent internalization pathway (De Tulleo 1998). This experimental data suggested that entry of HRV14 into endosomes is required for infection to occur. Using free-flow electrophoretic separation of microsomes, HRV14 was found to colocalize with the endosomal marker protein, horseradish peroxidase at 4°C, the temperature that prevent virus uncoating (Schober et al., 1998). The author also showed, with confocal microscope, that staining of HRV14 located to endosome. However, it raised the question of how ICAM-1 can associate with clathrin-coated vesicles in the absence of typical sorting signals recognized by APs (Staunton et al. 1988). The release of HRV14 genome is not dependent on endosomal acidification and results in endosome disruption. The chemical bafilomycin A specifically inhibits vacuolar H^+-ATPase and as the consequence, increases the intravascular pH to neutral. HRV14 was able to infect Hela cells under the condition of bafilomycin A suppressed endosome acidification, although the efficiency was reduced compared to control (Schober et al., 1998). When HRV14 was incubated with Hela cells at 37°C, no virus peak was found associated with endosomal material regardless of the

incubation time (Schober et al., 1998). This indicates that uncoating of HRV14 results in the disruption of endosome.

The release of virus genome requires a confirmation change in the capsid and generates two intermediate forms of subviral particles. Native poliovirus migrates at 150S in sucrose gradient and is hydrophilic, whereas subviral particles lacking of VP4 but with RNA sediment at 135S, and subviral particles which have lost of both VP4 and RNA at 80S. The 135S particles are hydrophobic due to the externalized N-terminus of VP1, which responsible for liposome attachment and proposed to form a pole in lipid membrane for RNA penetration (Fricks et al., 1990). Incubation of HRV14 and HRV3 with soluble ICAM-1 fragments results in formation of subviral particles and the transition occurs in a temperature dependent manner. At 37°C, HRV3 migrates to the position corresponding to 120S (saturated receptor binding form, with both VP4 and RNA) and to 80S (empty form) in the presence of ICAM-1, but sediments at 150S in the absence of ICAM-1 (Casasnovas and Springer 1994). With saturated receptor binding, HRV14 uncoated rapidly with a halftime [t½] = 2 h at 34°C, the optimal temperature for rhinoviruses propagation in cell culture. HRV3 had a halftime of 4 hours at 34°C while HRV16 exhibited very little uncoating under the same condition (Hoover-Litty and Greve 1993). The uncoating was not detectable at 4°C and 20°C for HRV3. At 37°C, HRV14 exhibited an uncoating halftime of 30 minutes. In contrast, the rate of formation of 135S particles was essentially identical at 34°C and 37°C. Rhinoviruses are sensitive to acidic condition (pH < 6). The virion rapidly becomes inactivated and disassembled when exposed to low pH. However, low pH does not work synergistically with ICAM-1 in promoting disruption of viral capsid in HRV3 (Casasnovas and Springer 1994). These data indicates an active role of ICAM-1 in the mediated the uncoating of HRV3 and HRV14.

The subviral particles representing poliovirus uncoating intermediates can be generated in vitro by incubating the virus at a temperature higher than 50°C in the presence of Ca^{2+}. A-particle sediments at 135S and appears hydrophobic, due to the exposure of VP1 protein and the release of VP4. The B-particles, which sediment at 80S, are an empty form that locks both VP4 and genome. The structures of the two intermediate forms were determined with cryo-electron microcopy and image reconstruction. Compared to the structure of native virion, an umbrella movement of VP1 to generate a channel between adjacent VP1 resulting in exposure of the internal peptide components (Belnap et al., 2000b). These data provide the first evidence of capsid transition to externalize internal peptides and genome. However there is still a lack of information on the role of receptor during virus uncoating. Some evidence supports and an active role of receptor in poliovirus uncoating. Entry of poliovirus was found to occur without endosomal acidification (Perez and Carrasco 1993). More direct evidence is that binding of receptor induces the disruption of poliovirus *in vitro* (Kaplan et al. 1990, 1991; Xing et al., 2000). Therefore, the best way to study viral uncoating is to investigate the capsid conformation of receptor-induced uncoating intermediates under physiological conditions.

2 AIM OF THE PROJECT

Cryo-electron microscopy (cryo-EM) is considered as one of the best tools to study the conformational changes during dynamic events such as receptor attachment and uncoating. By combining cryo-EM with x-ray crystallographic data, the interaction of viruses and their cognate receptor molecules can be elucidated with reasonable precision. The goal of my thesis was to reveal the structure-function relationships of picornaviruses with their cellular receptors during the early steps of viral infection. The results should enhance our understanding of viral infection mechanisms and perhaps provide new insights into prevention of viral disease. Specifically, this work focused on:

- Elucidating the mechanism of receptor recognition of picornaviruses with three related model systems: human echovirus 1 binding to integrin, and human poliovirus and human rhinoviruses with immunoglobulin receptors. The receptor interactions were studied by analyzing the structure of receptor-bound virus complex *in vitro*.

- Defining the dynamic events in receptor-mediated uncoating of human rhinoviruses. These dynamic events were studied in a time-resolving manner using virus-receptor complexes that were synthesized *in vitro*.

physiological temperature the receptor appears to bind to an open conformation of the canyon region, where contacts between protomers are loosened and internal polypeptides exposed. Binding of the receptor could then lock the protomers in their open conformation and generate minor rearrangements in the distribution of the different capsid proteins. The density clefts observed in the metastable virus-receptor complex $H3R^{H}$ could be used for RNA exit

4 GENERAL DISCUSSION:

The virus-receptor interaction is the first step in virus infection. Obviously, if the virus cannot bind to host cell, infection cannot be initiated and minimum effects on the cell are likely to result. The binding of the virus particle to the receptor involves numerous noncovalent interactions between the virus surface and the receptor, which leads to a specific, high-affinity interaction between a virus and a cell membrane molecule. Presumably, viruses have evolved to use receptors that are present on cells that have special features desired by virus. Thus, the binding to the receptor leads to i) virus entry, with the route determined by the action of the receptor; and ii) capsid uncoating, which is likely dependent on the RNA releasing site.

4.1.1 Receptor binding and virus entry

The most important role of a receptor is to function as the target for virus attachment, which results in viral infection. The notion that viruses require receptors for viral invasion came from the observation that human kidney and amnion, which were not normally infected by poliovirus, became highly susceptible to poliovirus when the cells were grown in culture (Kaplan et al. 1955). Later work found that this susceptibility correlated with the appearance of specific receptors on the cell surface, with the ability to bind and eclipse the virus (Holland 1959). Blocking of the receptor-binding site by either antibody or soluble receptor fragments inhibit virus infection. Transplantation of a receptor gene into non-susceptible cells allows for virus infection (Marjomäki et al., 2002).

Viruses may utilize the cell signal transportation route that has been established for the receptor. A good example of this is the entry of echovirus 1 (EV1). It has been reported that both α2 and β1 integrin subunits associated with caveolin-1 (Wary et al., 1998; Wei Y et al., 1996), the main protein component of caveolae. Caveolae refer to vesicles that have invaginated from cell membrane. The entry of echovirus-1 appeared to occur via caveolae endocytosis (Marjomäki et al., 2002), which is different from the entry of rhinoviruses, which occurs through clathrin-dependent endocytosis. EV1 infection was reduced by 66% when using Saos-α2β1 cells that express dominant negative caveolin, while EV1 infection has unaffected in wild type Saos-α2β1 cells. In EV1 infected Saos-α2β1 cells, both α2β1 integrin and virus were colocalized with coveolin-1, the caveolae presenting protein (Marjomäki et al., 2002). This observation suggests a tight association of α2β1 integrin and EV1 during the cell entry step. It was demonstrated that binding of α2I domain could stabilize viral capsid at 37°C (paper VII). That is probably due to the fact that α2β1 integrin is located in a raft-like membrane domain (Upla et al., 2002). The lipid composition is different in raft-like domain as compared to the regular cell membrane. Therefore, the stabilization of capsid by receptor binding ensures that the virus can be taken up into the cell with its genomic RNA intact.

Among the cell surface proteins, integrin is unique in its specific signaling function. The ligand integrin interaction can transduce signals cross the cell membrane, to trigger the change of integrin binding affinity (inside-out signaling), or to result in an intracellular response (outside-in signaling). The key question of activation of

Human echovirus 1 belongs to the genus of enteroviruses. α2β1 integrin binds to the south wall of the canyon. The receptor binding residues in EV1 are exposed and easily accessed. There is insufficient data available on the location of neutralization epitopes in EV1, even though pepscan result showed that anti-EV polyclonal antibody could recognize the VP1 C-terminus (T. Hyypia, personal communication). Integrin α2β1 can attach only to EV 1 and EV8, whereas these two viruses share the same antigenic epitopes and were even considered as the same virus (Melnick 1996). This fact suggests that the receptor is not favorable the selection of new serotypes.

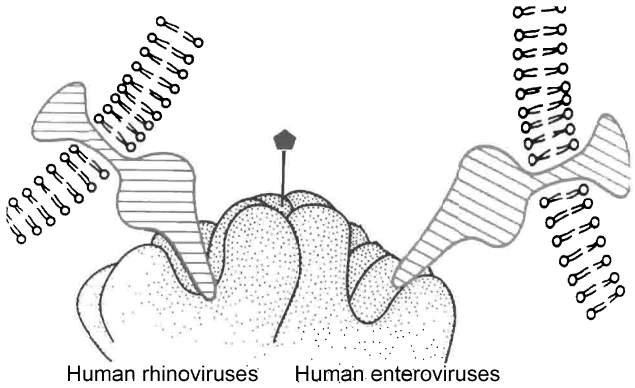

Figure 29: Schematic drawing of receptor binding in human rhinovirus and in human enterovirus. ICAM-1 inserts rather deeply into canyon and interacts with residues on the canyon floor, which are quite conservative among rhinovirus major group members. Receptors contact with the residues on the top region of canyon south wall, so that the receptor binding sites are partially overlapped with antigenic epitopes in the cases of human poliovirus and human echovirus 1.

4.1.5 Dynamic capsid behavior and viral uncoating

In contrast to the static view of the viral capsid that is given by x-ray crystallography, the capsid of picornaviruses is flexible and dynamic. VP4 and the N-terminus of VP1 are located at the internal surface of the capsid as determined by the crystal structure. However, antibodies against the N-terminal of VP1 or those against VP4 are able to precipitate poliovirus (Li et al., 1994). These antibodies only can bind when incubation takes place at 37°C. In HRV14, the internal peptides are accessible to an immobilized enzyme (Lewis et al., 1998). These data suggest a capsid-breathing hypothesis, i.e. the internal components of the capsid can be temporarily externalized, in a reversible manner. So far, there is no direct evidence about the capsid dynamics of EV1. However, the N-terminus of VP1 was recognized by antisera from rabbits that were immunized with native EV1 virion. These data suggest that the native virion exposes its internal peptide even though the capsid, at this stage, should be closed in order to protect the genome.

HRV3 uncoating requires a receptor-catalyzed capsid expansion, which generates holes in the capsid for the exit of the viral genome. Our study reveals for the first time that capsid expansion could be substantially induced by receptor binding at physiological temperatures and, therefore, it might occur during virus entry. No viral capsid expansion was observed in HRV16-receptor complexes, a serotype with

pocket-factor molecules expected to inhibit capsid dynamics or breathing (Lewis et al., 1998). This observation, together with the dependence of rhinovirus uncoating with temperature, suggests that particle expansion requires capsid breathing. Therefore, rather than being the trigger of the expansion, the binding of the receptor molecules could mainly help holding the capsid in an expanded state by simultaneous binding to two neighboring capsid protomers. It is not clear whether the expansion could be just localized within the two receptor-interacting protomers or would need the synchronized expansive movement of at least the five-fold related protomers within a pentamer. However, reported by Hoover-Litty and Greve, uncoating is receptor-concentration dependent and is favored by maintaining sufficient levels of receptor binding on the virus capsid (Hoover-Litty and Greve 1993). It is likely that the binding of multiple receptors at a few continuous protomers is necessary for marinating the capsid at an open state.

In the expanded capsid, the excess density seen in H3Rh particles indicated the putative sites for the internal peptides to exit. Such density was found nearby the protomer interface probably contributed by the externalized N-terminal loop of VP1. The N-termini of VP1 located underneath the protomer interface next to a channel at the junction between the canyon floor and the south wall. The position of this density bridged the receptor and canyon north wall. Thus, the bound receptor molecules might incorporate with the externalized peptides to arrest the capsid at an expansion state (Fig. 28). In addition, VP1 was reported to associate with C-terminal VP4 through a highly conserved motif (1032-1042). A point mutation at this motif was recently reported to alter the formation rate of VP4-lacking particles in coxsackievirus A9 (Airaksinen et al. 2001). Thus, VP4 might leave the virion through the same channel. As the VP4 and the RNA were found to release simultaneously from HRV3 virion (Casasnovas and Springer 1994), it is likely that RNA uses the same exit as well.

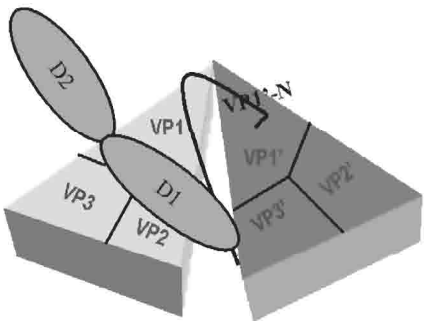

Figure 30: The dynamic feature of virus capsid reversibly exposes the N-terminal of VP1, which appears to locate internally in the crystal structure. The ICAM-1 binding on HRV3 function as locker to stabilize the viral capsid at expanded condition, so that the uncoating goes irreversible.

The RNA release of picornaviruses has been suggested to occur through one of its 12-pentameric vertices. However, there has not been any evidence showing the exposure of VP3 N-terminal cylinder plugging above VP4 N-terminal at fivefold axis (Fig 8). Analyses of uncoating intermediates in HRV3 and in poliovirus demonstrated little evidence in seeing any capacious tunnel through the fivefold conjunction among the VP1s to be the RNA exit. Instead, the readily seen cleft, at the junction between canyon floor and the south wall, was more likely to be the passage for the internal peptides and genome to be released. The excess density seen in $H3R^{H}$ nearby the cleft further confirmed such location. Nevertheless, uncoating of poliovirus was lately

observed at 4°C when a mutation was induced at the residues around this region at protomer interface (I Pelletier and F Colbere-Garapin, personal communication).

In conclusion picornavirus uncoating can be described using the thermodynamic model (Fig 31). A relative large energy boundary (Eα) separates the native virion and the uncoated particle. Energy is required by both conformational change of the virus capsid and the subsequent release of RNA genome. The presence of capsid breathing indicates that energy requirement for capsid conformational change is not large. The energy needed for RNA release is so great that, together with the internal proteins, the RNA genome cannot be exposed before accomplishing infection. In fact, the intact virions were found to be infectious after RNase treatment from the purification process. Binding of receptor lowers energy boundary, which in turn enhances the feasibility of viral uncoating (Tsang, et al. 2001). Without the receptor, virus alone has to be heated to 55°C to release the genomic RNA, but with receptor binding, viral uncoating can occur at 30°C in HRV3. The mechanism of receptor binding and concomitant reduction of the energy boundary has not been clear defined. In our study, capsid expansion occurred when HRV3 attached to ICAM-1 at physiological conditions. Thus the bound receptor may serve as wedge to hold capsid in an opening confirmation. The bound receptor may also contact the externalized VP1-N-termini and VP4. Since HRV3-ICAM-1 empty particle demonstrates that further stages of capsid conformational change are necessary, compared to the capsid of RNA containing HRV3-ICAM-1 particles, the bound receptor could participate with viral proteins to overcome such changes.

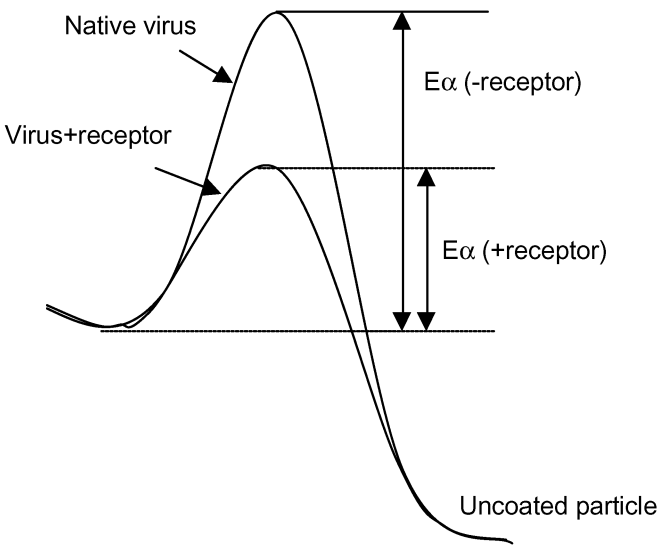

Figure 31: Graphic representation of a thermodynamic model for virus uncoating (Smith et al., 2001)

5 ACKNOWLEDGEMENTS

During my study, I have got lots of help from the people in the department and my friends. I would like to address my sincere thanks:

To my supervisor, **Holland Cheng**, for creating a stimulating working environment. I most appreciate his endless support in discovering my potential from the first interview. I enjoy very much every discussion point with him in good times and bad times of my thesis projects. Over the years of study, I have been very much inspired by his enthusiasm about Science and thus believe that to continue working in Science is indeed joyful.

To **Henrik Garoff**, for bringing a crystal-pure academia in the department

To **Jose Casasnovas,** for his fine skills in biochemistry in both poliovirus and rhinovirus work.

To my collaborators in Finland, especially **Mikko Huhtala, Vilja Pietiainen**. I enjoy the Picorna-network meeting very much and, of course, the Finnish sauna.

To **Kerstin Forsell**, for the collaboration.

To **Birgitta Lindqvist**, for the collaboration**.**

To **Lena Hammar**, for taking care of me at both Christmas and midsummer, and for her endless stories on both Swedish culture and tradition.

To **Lars Haag**, for sharing the office and for solving computer troubles together.

To **Josefina Nilsson**, for nice companion in Paris during the international congress in Virology.

To **Fredrik Sjöborg**, for driving us to SBNet meeting.

To **Willem van de Beek**, I wish him good luck.

To **Leif Bergman**, for his excellent programming work.

To **Bomu Wu**, for teaching me about icosahedral symmetry and common-lines.

To **Sevak Markarrian**, for his help.

To **Naoyoki**, **Miyazaki** for his visit, from which I learned crystallographic programs.

To **Jan, Sedzik**, for crystallizing Li's virus.

To **Maarit Suomalainen** for the fruitful discussions.

To **Kjell Hultenby** for allowing me pumping my cryo-holder in your lab, which is

strong base of my cryo-EM work.

To **Erik Lundgren** for handling the entire Novum network, which, in my opinion, is really difficult.

To **Gudran Tibbelin** for her friendship and for the supports.

To the people in the department for the nice working environment. And to the people in the administration for their help.

To my best friend, **Hongxing Zhao**. For the friendship and encouragement, which are the strong supports for me. And to her family, **Jane and Min Pan**, for all the parties we had together.

To **Helena Ström,** cheers.

To my friends, **Li Liu** and **Lei Luo**, for all the midsummer parties.

To my husband, **Lijun Ma,** for his understanding and patience.

To my brother, **Jian Xing**, for always being there and for holding me at the most difficult time in our life.

To my daughter, **Xiao Ma**, for her understanding and for the time without mother around. "*I miss you so much and I love you…*"

To my father, **Yulong Xing**, for building the wish of learning in me, for his endless support in my life. This thesis would not be completed without his contribution.

I devoted this thesis to my mother, **Hongluan Guo**. Without her support, I could never come so far to the position I am standing now. I do not think any words in the world could describe what she means to me. What I know is that she was always there with me at every moment of my life, and she will be there with me for the rest of my life.

If I miss anyone here, that was not my intention and I am so sorry for that.

6 REFERENCES

Adrian M, D. J., Lepault J and Mcdowall, AW (1984). "Cryo-electron microscopy of viruses." Nature **308**: 32-36.

Airaksinen, A., Roivainen M, and Hovi T. (2001). "Coxsackievirus A9 VP1 mutants with enhanced or hindered A particle formation and decreased infectivity." J Virol **75**(2): 952-60.

Akula S. M., Pramod N. P., et al. (2002). "Integrin alpha3beta1 (CD 49c/29) is a cellular receptor for Kaposi's sarcoma-associated herpesvirus (KSHV/HHV-8) entry into the target cells." Cell **108**(3): 407-19.

Baker, T. S. and Cheng. R.H. (1996). "A model-based approach for determining orientations of biological macromolecules imaged by cryoelectron microscopy." J Struct Biol **116**: 120-130.

Belnap, D., McDermott B. M., Jr. et al. (2000a). "Three-dimensional structure of poliovirus receptor bound to poliovirus." Proc Natl Acad Sci U S A **97**(1): 73-8.

Belnap, D. M., Filman, D. J. et al. (2000b). "Molecular tectonic model of virus structural transitions: the putative cell entry states of poliovirus." J Virol **74**(3): 1342-54.

Belnap DM, Kumar A., et al. (1999). "Low-resolution density maps from atomic models: how stepping "back" can be a step "forward"." J Struct Biol **125**(2-3): 166-175.

Bergelson, J. M., Chan, B. M. et al. (1993). "The integrin VLA-2 binds echovirus 1 and extracellular matrix ligands by different mechanisms." J Clin Invest **92**(1): 232-9.

Brunger, A. T. (1992). X-PLOR, version 3.1. A system for X-ray crystallography and NMR, Yale University Press, New Haven, CT.

Casasnovas, J. M. and Springer T. A. (1994). "Pathway of rhinovirus disruption by soluble intercellular adhesion molecule 1 (ICAM-1): an intermediate in which ICAM-1 is bound and RNA is released." J Virol **68**(9): 5882-9.

Casasnovas, J. M. and Springer T. A. (1995). "Kinetics and thermodynamics of virus binding to receptor. Studies with rhinovirus, intercellular adhesion molecule-1 (ICAM-1), and surface plasmon resonance." J Biol Chem **270**(22): 13216-24.

Casasnovas, J. M., Stehle T., et al. (1998). "A dimeric crystal structure for the N-terminal two domains of intercellular adhesion molecule-1." Proc Natl Acad Sci U S A **95**(8): 4134-9.

Casjens, S. (1997). Principles of virion structure, function, and assembly. Structural Biology of Viruses. W. Chiu, Burnett RM, Garcea RL. New York, Oxford University Press Inc.**:** 3-37.

Caspar, D. L. D. (1956) "The Sructure of Bushy Stunt Virus." Nature *177*, 475-476.

Caspar D and Klug A. (1962). "Physical principles in the construction of regular viruses." Cold Spring Harbor Symp. Quant. Biol. **27**: 1-24.

Che, Z., Olson, N. H. et al. (1998). "Antibody-mediated neutralization of human rhinovirus 14 explored by means of cryoelectron microscopy and X-ray crystallography of virus-Fab complexes." J Virol **72**(6): 4610-22.

Cheng RH, Reedy V et al. (1994). "Functional implications of quasi-equivalence in a T = 3 icosahedral animal virus established by cryo-electron microscopy and X-ray crystallography." Structure **2**(4): 271-282.

Colonno RJ, Callahan PL, and Long WJ. (1986). "Isolation of a monoclonal antibody that blocks attachment of the major group of human rhinoviruses." J Virol **57**: 7-12.

Crick F and Watson, J. (1956). "The structure of small viruses." Nature **177**: 473-475.

Crowther RA (1971) Procedures for three-dimensional reconstruction of spherical viruses by Fourier synthesis from electron micrographs. Philos Trans R Soc Lond B Biol Sci. 261:221-30.

De Tulleo, L. and Kirchhausen, T. (1998). "The clathrin endocytic pathway in viral infection." EMBO J **17**: 4584-4593.

Dickeson, S. K., Mathis, N. L. et al. (1999). "Determinants of ligand binding specificity of the alpha(1)beta(1) and alpha(2)beta(1) integrins." J Biol Chem **274**(45): 32182-91.

Dubochet J, Adrian M., et al. (1988). "Cryo-electron microscopy of vitrified specimens." Q. Rev. Biophys. **21**: 129-228.

Dubochet J and Adrian M (1981). "Vitrification of pure water for electron microscopy." J Microsc **124**: RP3-RP4.

Emsley, J., King, S. L et al. (1997). "Crystal structure of the I domain from integrin alpha2beta1." J Biol Chem **272**(45): 28512-7.

Emsley, J., Knight C. G., et al. (2000). "Structural basis of collagen recognition by integrin alpha2beta1." Cell **101**(1): 47-56.

Enders, J., Weller TH, and Robbins FC. (1949). "Cultivation of the Lansing strain of poliomyelitis virus in cultures of various human embryonic tissues." Sciences **109**: 85-87.

Erickson HP, and Klug A. (1971). "Measurement and compensation of defocusing and aberations by Fourier processing of electron micrographs." Phil., Trans. Roy. Soc. Lond. B. **261**: 105-118.

Filman, D., Wien MW, et al. (1998). "Structure determination of echovirus 1." Acta Crystallogr. D. **54**: 1261- 1272.

Fricks, C. E. and Hogle, J. M. (1990). "Cell-induced conformational change in poliovirus: externalization of the amino terminus of VP1 is responsible for liposome binding." J Virol **64**(5): 1934-45.

Hadfield, A. T., Lee, W. et al. (1997). "The refined structure of human rhinovirus 16 at 2.15 A resolution: implications for the viral life cycle." Structure **5**(3): 427-41.

Harber J., Bernhardt G., et al. (1995). "Canyon rim residues, including antigenic determinants, modulate serotype-specific binding of polioviruses to mutants of the poliovirus receptor." Virology **214**(2): 559-70.

Hawkes, P. (1991). Image Formation and Contrast. Biophysical Electron Microscopy: Basic concepts and Modern Techniques. H. P. a. V. U, Academic Press**:** 89-108.

He, Y., Chipman P.R., et al. (2001). "Interaction of coxsackievirus B3 with the full length coxsackieviru-adenovirus receptor." Nature Struc Biol **8**(10): 874-878.

He Y., Bowman V. et al. (2000). "Interaction of the poliovirus receptor with poliovirus." Proc Natl Acad Sci U S A **97**: 79-84.

Hogle, J. M., Chow, M. et al. (1985). "Three-dimensional structure of poliovirus at 2.9 A resolution." Science **229**(4720): 1358-65.
Holland, J. (1959). "The mammalian cell-virus relationship. II. Adsorption, reception and eclipse of poliovirus by Hela cells." J Exp Med **109**: 487-504.
Holland, J. J. (1962). "Irreversible eclipse of poliovirus by Hela cells." Virology **16**: 163-176.
Hoover-Litty, H. and J. M. Greve (1993). "Formation of rhinovirus-soluble ICAM-1 complexes and conformational changes in the virion." J Virol **67**(1): 390-7.
Hopper P, H. S., Sauer RT (1984). "Structure of tomato bushy stunt virus: coat protein sequence determination and its structural implications." J Mol Biol **177**: 701-713.
Ivaska, J., L. Nissinen, et al. (2002). "Integrin alpha 2 beta 1 promotes activation of protein phosphatase 2A and dephosphorylation of Akt and glycogen synthase kinase 3 beta." Mol Cell Biol **22**(5): 1352-9.
Ivaska, J., Reunanen H., et al. (1999). "Integrin alpha2beta1 mediates isoform-specific activation of p38 and upregulation of collagen gene transcription by a mechanism involving the alpha2 cytoplasmic tail." J Cell Biol **147**(2): 401-16.
Johnson, J. E. and Speir, J.A. (1997). "Quasi-equivalent viruses: a paradigm for protein assemblies." J Mol Biol **269**: 665-675.
Kamata, T., Liddington, R. C. et al. (1999). "Interaction between collagen and the alpha(2) I-domain of integrin alpha(2)beta(1). Critical role of conserved residues in the metal ion-dependent adhesion site (MIDAS) region." J Biol Chem **274**(45): 32108-11.
Kaplan, A. S. (1955). "The susceptibility of monkey kidney cells to poliovirus in vivo and in vitro." Virology **1**: 377-392.
Kaplan, G. G. Peters, D. and Racaniello V.R. (1990). "Poliovirus mutants resistant to neutralization with soluble cell receptors." Science **250**: 1596-1599.
King, S. L., Kamata, T. et al. (1997). "Echovirus 1 interaction with the human very late antigen-2 (integrin alpha2beta1) I domain. Identification of two independent virus contact sites distinct from the metal ion-dependent adhesion site." J Biol Chem **272**(45): 28518-22.
Klug, A., Finch J. T. and Franklin R. E. (1957). The structure of Turnip Yellow mosaic virus: X-ray diffraction studies. Biochim. et Biophys. Acta., 25: 242-252.
Knight, C. G., Morton, L. F. et al. (2000). "The collagen-binding A-domains of integrins alpha(1)beta(1) and alpha(2)beta(1) recognize the same specific amino acid sequence, GFOGER, in native (triple-helical) collagens." J Biol Chem **275**(1): 35-40.
Kolatkar, P. R., Bella J., et al. (1999). "Structural studies of two rhinovirus serotypes complexed with fragments of their cellular receptor." EMBO J **18**: 6249-59.
Lewis, J. K., Bothner, B. et al. (1998). "Antiviral agent blocks breathing of the common cold virus." Proc Natl Acad Sci U S A **95**(12): 6774-8.
Mancini EJ, de Haas F, and Fuller SD (1997). High-resolution icosahedral reconstruction: fulfilling the promise of cryo-electron microscopy. Structure 5:741-50.

Li, Q., Yafal, A. G. et al. (1994). "Poliovirus neutralization by antibodies to internal epitopes of VP4 and VP1 results from reversible exposure of these sequences at physiological temperature." J Virol **68**(6): 3965-70.
Liddington R, Yan, Y. et al. (1991). "Structure of simian virus 40 at 3.8Å resolution." Nature **354**: 278-284.
Liljas L, Unge, T. et al. (1982). "Structure of satellite tobacco necrosis virus at 3.0Å resolution." J Mol Biol **159**: 93-108.
Luo M, Vriend, G. et al. (1989). "Structure determination of Mengo virus." Acta Crystallogr B **45**: 85-92.
Marjomäki, V., Pietiäinen V, et al. (2002). "Internalization of Echovirus 1 in caveolae." J Virol **76**(4): 1856-1865.
Melnick, J. L. (1996). Enteroviruses: polioviruses, coxsackieviruses, echoviruses, and newer enteroviruses. Fields Virology. K. D. Fields BN, Howley PM. Philadelphia, Lippincott-Raven.
Miller, L. C., Blakemore W., et al. (2001). "Role of the cytoplasmic domain of the beta-subunit of integrin alpha(v)beta6 in infection by foot-and-mouth disease virus." J Virol **75**(9): 4158-64.
Mineo, C., Ying YS, et al. (1998). "Targeting of protein kinase Calpha to caveolae." J Cell Biol **141**(3): 601-10.
Norkin LC, Anderson, H. et al. (2002). "Caveolar endocytosis of simian virus 40 is followed by brefeldin A-sensitive transport to the endoplasmic reticulum, where the virus disassembles." J Virol **76**: 5156-5166.
Olson, A.J., Bricogne G, and Harrison SC. (1983). "Structure of tomato bushy stunt virus IV: the virus particle at 2.9Å resolution." J Mol Biol **171**: 61-93.
Olson, N. H., Kolatkar, P. R. et al. (1993). "Structure of a human rhinovirus complexed with its receptor molecule." Proc Natl Acad Sci U S A **90**(2): 507-11.
Palmenberg, A. C. (1989). Sequence alignments of Picornaviral Capsid Proteins. Molecular Aspects of picornaviruses infection and detection. American society for microbiology, Washington DC.
Parry N, Fox, G. et al. (1990). "Parry N, Fox G, Rowlands D, Brown F, Fry E, Acharya R, Logan D, Stuart D." Nature **347**: 569-572.
Pentikainen, O., Hoffren, A. M. et al. (1999). ""RKKH" peptides from the snake venom metalloproteinase of Bothrops jararaca bind near the metal ion-dependent adhesion site of the human integrin alpha(2) I-domain." J Biol Chem **274**(44): 31493-505.
Perez, L. and Carrasco L. (1993). "Entry of poliovirus into cells does not require a low-pH step." J Virol **67**(8): 4543-4548.
Racaniello, V. R. (1996). "Early events in poliovirus infection: virus-receptor interactions." Proc Natl Acad Sci U S A **93**(21): 11378-81.
Robinson, I. and Harrison, S. (1982). "Structure of the expanded state of tomato bushy stunt virus." Nature **297**: 563-568.
Rossmann, M. G., Arnold E. et al. (1985). "Structure of a human common cold virus and functional relationship to other picornaviruses." Nature **317**(6033): 145-53.
Rueckert, R. (1996). Picornaviridae: the viruses and their replication. Field Virology, 3rd ed. K. D. Fields BN. New York, Raven Press.
Rueckert, RR, D. A., and Stoltzfus CM (1969). "The structure of Maus-Elberfeld virus; a model." Proc Natl Acad Sci USA. **62**: 912-929.

Schober, D., P. Kronenberger, et al. (1998). "Major and minor receptor group human rhinoviruses penetrate from endosomes by different mechanisms." J Virol **72**(2): 1354-64.

Selzer T., Albeck, S., and Schreiber G. (2000). "Rational design of faster associating and tighter binding protein complexes." Nat Struct Biol **7**(7): 537-541.

Selzer T., and Schreiber G. (1999). "Predicting the rate enhancement of protein complex formation from the electrostatic energy of interaction." J Mol Biol **287**: 409-419.

Sherry, B., Mosser, A. G. et al. (1986). "Use of monoclonal antibodies to identify four neutralization immunogens on a common cold picornavirus, human rhinovirus 14." J Virol **57**(1): 246-57.

Sherry, B and Rueckert, RR (1985). "Evidence for at least two dominant neutralization antigens on human rhinovirus 14." J Virol **53**(1): 137-43.

Sixma, J., van Zanten GH et al. (1997). "Platelet adhesion to collagen: an update." Thromb Haemost **78**(1): 434-438.

Smart, E. J., Foster, D. C. et al. (1994). "Protein kinase C activators inhibit receptor-mediated potocytosis by preventing internalization of caveolae." J Cell Biol **124**(3): 307-13.

Solecki D, Gromeier, M. et al. (1998). "Poliovirus and its cellular receptor: a molecular genetic dissection of a virus/receptor affinity interaction." J Mol. Recogn. **11**: 2-9.

Staunton D. E., Dustin, M. L. et al. (1990). "The arrangement of the immunoglobulin-like domains of ICAM-1 and the binding sites for LFA-1 and rhinovirus." Cell **61**(2): 243-54.

Staunton, D. E. Marlin, S.D. et al. (1988). "Primary structure of ICAM-1 demonstrates interaction between members of the immunoglobulin and integrin supergene families." Cell **52**: 925-933.

Tsang, S. K., McDermott, B. M. et al. (2001). "Kinetic analysis of the effect of poliovirus receptor on viral uncoating: the receptor as a catalyst." J Virol **75**(11): 4984-9.

Upla, P., Marjomäki V, Kankaanpää P, Hyypiä T, van der Goot FG and Heino J (2002). "Integrin clustering targets echovirus 1 to caveolae and activates internalization." personal communication.

van der Saag, P., Caldenhoven E, and van de Stolpe A. (1996). "Molecular mechanisms of steroid action: a novel type of cross-talk between glucocorticoids and NF-kappa B transcription factors." Eur Respir J Suppl: 146s-153s.

Wang, J. (2002). "Protein recognition by cell surface receptors: physiological receptors versus virus interactions." Trends Biochem Sci **27**(3): 122-126.

Wary KK, Mariotti, A. et al. (1998). "A requirement for caveolin-1 and associated kinase Fyn in integrin signaling and anchorage-dependent cell growth." Cell **94**: 625-634.

Wei Y, Lukashev, M. et al. (1996). "Regulation of integrin function by the urokinase receptor." Science **273**: 1551-1555.

Xing, L., Tjarnlund K. et al. (2000). "Distinct cellular receptor interactions in poliovirus and rhinoviruses." EMBO J **19**(6): 1207-16.

Xiong, J., Stehle T, et al. (2001). "Crystal structure of the extracellular segment of integrin αVβ3." Science **294**: 339-345.

Xu J, C. R. (1997). "A three-dimensional collagen lattice induces protein kinase C-ζ activity: role in α2 integrin and collagenase mRNA expression." J Cell Biol **136**: 473-483.

Zemlin, F. (1994). "Expected contribution of the field-emission gun to high-resolution transmission electron microscopy." Ultramicroscopy **25**(3): 223-226.

Zhao, R., Pevear, D. C. et al. (1996). "Human rhinovirus 3 at 3.0 A resolution." Structure **4**(10): 1205-20.